Porous-layer model for laminar liquid flow in rough microchannels

S. Izquierdo*

Dipartimento di Energetica, Politecnico di Torino,
Corso Duca degli Abruzzi 24, 1019 Torino, Italy and
Instituto Tecnológico de Aragón (ITA),
María de Luna 8, 50018 Zaragoza, Spain

M. Martínez and J.R. Valdés†

Instituto Tecnológico de Aragón (ITA),
María de Luna 8, 50018 Zaragoza, Spain

M. Accolti

Instituto Tecnológico de Aragón (ITA),
María de Luna 8, 50018 Zaragoza, Spain and
Dipartimento di Energetica, Politecnico di Torino,
Corso Duca degli Abruzzi 24, 1019 Torino, Italy

S. Woudberg and J.P. Du Plessis

Department of Mathematical Sciences, University of Stellenbosch,
Bag X1 Matieland 7602, South Africa

P. Asinari

Dipartimento di Energetica, Politecnico di Torino,
Corso Duca degli Abruzzi 24, 1019 Torino, Italy

(Dated: December 23, 2009)

Abstract

A reduced description of the three-dimensional effects of rough surfaces on the laminar liquid flow in microchannels is sough. With this outlook a one-dimensional model is proposed, which is built by splitting the channel in two regions: porous and fluid. The porous one is a layer fixed to the wall and represents the roughness. Special attention is paid to three aspects not fully solved in previous porous-layer approaches recently proposed. These are: (i) a complete and unified derivation of the porous-layer model through spatial averaging; (ii) the development of a physically sound stress model for the porous region only as a function of the geometrical characteristics of the roughness; and (iii) the derivation of an appropriate treatment of the interface fluid-porous. The development of this generalized porous-layer model has two objectives: to provide simple and accurate models for lump simulation tools; and to get insight into the physic of the liquid flow at rough interfaces in microchannels. The stress model in the porous layer, the slip boundary condition at the interface and the porous-layer model are validated against numerical simulations and experimental data from the bibliography. Additionally, further validation using numerical simulation of wavy, cube- and pyramid-based rough channels is performed. Results show that the porous-layer model is valid to approximate the three-dimensional solution of any connected rough surface with an error below 10% for the following conditions: relative roughness $k/H < 0.5$, relative width $L/H < 30$ and porosity $\varepsilon < 0.8$. The validation is restricted to very low Reynolds number. It is expected that, due to the fundamental derivation of the method, it can be extended to model advanced fluid flow effects in microchannels.

*Electronic address: salvador.izquierdo@polito.it

†Electronic address: jrvaldes@ita.es

I. INTRODUCTION

The knowledge about the effect of roughness on laminar fluid flow in microchannels is continuously increasing due to recent numerical results and also, and mainly, due to improved experimental techniques which help us to obtain accurate description of the behavior of the fluid flow at microscales [16, 44]. Thus, consistent simplified models can be formulated to include these effects when performing multiscale simulations of complex industrial system that include any kind of fluid flow through a rough microchannel, such as hydrodynamic lubrication processes [13, 35], microhydraulic systems or MEMS [9]. Simple microfluidic models of rough channels can be useful for lump modeling of industrial complex systems, for simplified analysis of complicated 3D flows in microfluidics applications, or as an approach to define equivalent slip boundary conditions to reproduce roughness effects.

A reduced order model developed to reproduce fluid flow in rough microchannels should be physically sound, based on first principles and, ideally, analytical. Additionally, it should be valid for any kind of fluid, for a wide range of Reynolds numbers, and for any roughness height and any rough geometry (even anisotropic ones). Some further desirable properties would include the ability for reproducing surface phenomena as hydrophobic and hydrophilic effects, and the ability to provide information about force decomposition (as it can be obtained from a 3D CFD simulation). If the method is not analytical it would be desirable having a simple and computationally cheap one in order to reduce as much as possible the complexity of the implementation.

A review is presented in Table I of available approaches to perform simplified or analytical analysis of the influence of roughness in channels. The objective of this review is to identify the approach that can better provide the above-mentioned characteristics when modeling the laminar fluid flow in rough microchannels, which is mainly characterized by high relative roughness. The first approach in Table I is the classical hydraulic engineering approach, which consider the roughness through a friction factor or a resistance coefficient obtained experimentally or numerically (using 2D/3D CFD simulations). The basic approach [6, 22, 25] provides a general description of laminar and turbulent flows within rough conduits. It is only valid for roughness up to 5%. Generalizations of the Moody chart [12, 15] provide and improved description for high relative roughness in laminar and turbulent flows. Additionally to the friction factors, it is also possible to define resistance coefficients from CFD

Approach	**Method**	**Dim.**
Friction factor	Moody chart [6, 22, 25]	0D
	Moody chart generalization [12, 15]	0D
	Resistance coefficient [36, 37]	0D
Modified boundary conditions	Modified slip [29, 32]	1D-2D
	Perturbation methods [32, 41]	1D-2D
	Stochastic slip [5, 5]	0D
Effective viscosity	Roughness viscosity model [21]	1D-(2D)
Layer models	Porous-media layer [19, 20]	1D-(2D)
	Rough-layer model [2, 10]	1D-(2D)
Asymptotic analysis	Stokeslet [11, 27]	2D-3D
	Eigenfunction expansion [18, 31, 40]	2D-3D

TABLE I: Reduced-order approaches to evaluate or describe the influence of roughness in channels. The last column is the dimension of the model.

simulations [36, 37]. A second possible approach is the definition of a modified boundary condition. It is typically a Neumann or a Robin condition at the boundary that generates a positive or negative slip equivalent to the particular effect studied at the wall [29, 32]. This modified slip boundary condition is applied in a fictitious wall with a location depending on the roughness. An equivalent extrapolated non-slip condition can be defined. Contributions to this approach include: perturbation methods [32, 41], which have been derived for some grooved surfaces and are limited to shallow elements; and the stochastic slip boundary condition [5, 5], which take into account the formation of nano-bubbles at the wall. In the latter approach, the actual slip length is based on the mean roughness, the spatial autocorrelation and the fraction of bubbles at walls. Alternatively to boundary-condition modification, a modified fluid flow behavior can be introduced through a change of the viscosity as a function of the distance to the wall [21]. However, with these two approaches (modified boundary condition and modified viscosity) we loss information about the velocity profile within the microchannel, which can be of interest for some application (*eg* mixed lubrication processes). A fourth approach is build by splitting the domain in two layers, one for the laminar fluid flow and the other for taken into account the roughness effects. For this case,

the resistance speed factor can be obtained from experimental correlations, and porous media parameters adjusted to fit experimental data [19, 20]. Alternatively, the needed input information can came from numerical data by computing the drag in the rough layer from 2D and 3D CFD simulations [2, 10]. Finally, an available fifth approach joint those methods based on computing asymptotic solutions for the Stokes flow. The Stokeslet fundamental solution method [11, 27] provide arbitrary accurate solutions but usually based on numerical approaches. The eigenfunction expansion method [18, 31, 40] has the advantage that it can be extended for any kind of geometry, but for complex ones a numerical approach is compulsory.

Looking for a reduced-order method in Table I and attending to the ideal properties described above, we conclude that the layer method are those that can better reproduce the fluid flow behavior without losing relevant information. This approach is a well-balanced trade-off between simplicity (one-dimensional approach) and accuracy (it is derived by averaging of the three-dimensional equations). Furthermore, the structure of the approach would allow moving to a two-dimensional approach if more complex phenomena are needed to be simulated.

An additional aspect to be discussed when analyzing the fluid flow over rough walls is the appropriate characterization of these surfaces. For the study of the influence of roughness in the flow, synthetic surfaces are preferred to real ones due to the possibility of controlling geometrical parameters. Synthetic surfaces can be roughly classified as: (a) roughness build with geometric elements (*eg* prisms, pyramids, wavy patterns or spheres) arranged in several ways (aligned, staggered or random) and with fluid connectivity through the rough area; (b) patterns with grooves or dimples without fluid connection between them; and (c) self-affine fractal roughness to reproduce surfaces with natural growing mechanisms (*eg* nucleation or fracture). In this work we only consider geometries falling into the first group.

The generalized transport equations, which are the basis for the porous layer model, are introduced in Sec. II. In Sec. III a one-dimensional porous layer model is obtained and analyzed under some restrictions and assumptions. The resulting model is based on a previous model recently developed [10], which is here improved by rigorously derived the average equations [26] and by computing, from a simple geometrical procedure, the stress tensor in the porous layer [43], avoiding any input from numerical or experimental data. Once

the equation of the model is set, two alternative strategies for solving it are described in Secs. IV and V. The porous layer model introduced is validated in Sec. VI using experimental and numerical data from the bibliography and with original CFD simulation of several kinds of synthetic roughness. Finally, in Sec. VII conclusions are drawn and possible extensions are discussed.

II. GENERALIZED TRANSPORT EQUATIONS

The averaged transport equations are here derived for the fluid flow of the α-phase in a channel at the steady state (see Fig. 1).

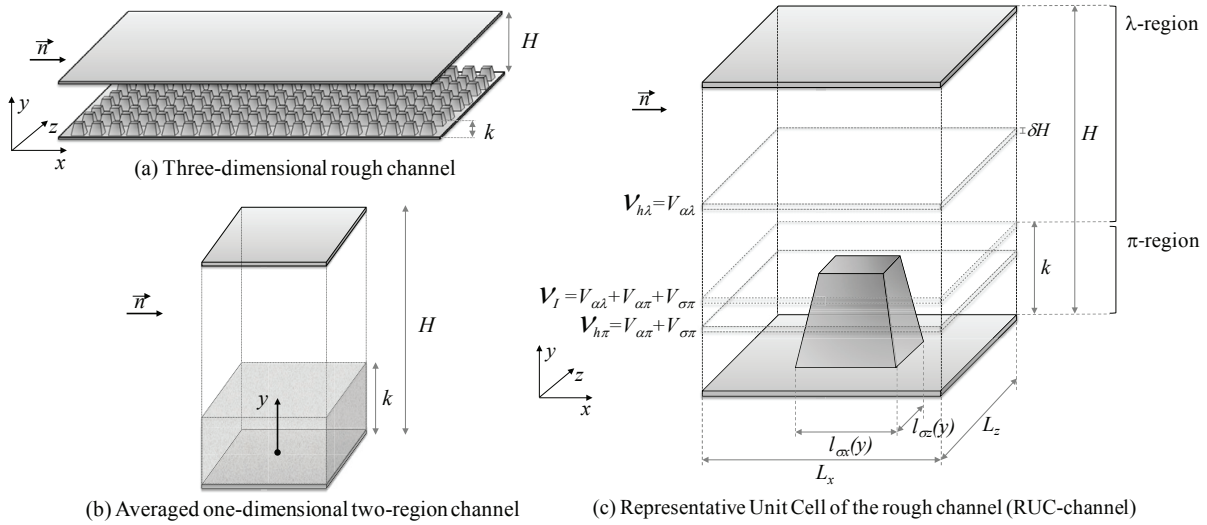

FIG. 1: Schematic description of the geometry considered for describing the generalized transport equations.

The channel has a homogeneous fluid λ–region and a homogenous porous π–region with a fluid-porous λ-π–interface between regions. In the homogeneous regions the fluid is assumed to be not affected by rapid variation of properties occurred in boundary regions. The flow is considered incompressible and inertial effects are neglected. Therefore, we start the description of the method with the three-dimensional incompressible Stokes system of equations for the fluid α–phase at the steady state within the whole domain:

$$\nabla \cdot \mathbf{u}_\alpha = 0; \tag{1}$$

$$0 = -\nabla p_\alpha + \mu_\alpha \nabla^2 \mathbf{u}_\alpha + \mathbf{f}_\alpha; \tag{2}$$

where $\mathbf{u}_\alpha$ is the velocity vector, p_α is the pressure, μ_α is the viscosity and $\mathbf{f}_\alpha$ is a body force. For solving this system of equations the no-slip boundary condition is set at the α–fluid-phase and σ–solid-phase interface:

$$\mathbf{u}_\alpha\big|_{\alpha\sigma} = 0; \tag{3}$$

and also at upper and bottom walls:

$$\mathbf{u}_\alpha\big|_{y=0} = 0; \tag{4}$$

$$\mathbf{u}_\alpha\big|_{y=H} = 0. \tag{5}$$

To account for the porous media description the superficial volume average of a quantity ϕ_α is defined in the α-phase as:

$$\overline{\phi}_\alpha = \frac{1}{\mathcal{V}} \int_{V_\alpha} \phi_\alpha dV; \tag{6}$$

and the intrinsic volume average:

$$\overline{\phi}_{\alpha,\bar{\alpha}} = \frac{1}{V_\alpha} \int_{V_\alpha} \phi_\alpha dV. \tag{7}$$

The relation between superficial an intrinsic volume average quantities is:

$$\overline{\phi}_\alpha = \varepsilon_\alpha \overline{\phi}_{\alpha,\bar{\alpha}}. \tag{8}$$

being ε_α the porosity for the α-phase defined as:

$$\varepsilon_\alpha = \frac{V_\alpha}{\mathcal{V}}. \tag{9}$$

Considering the geometry in Fig. 1(c), $L = L_x = L_z$ and $l_\sigma = l_{\sigma x} = l_{\sigma z}$, and only one-phase fluid flow, the porosity would be $\varepsilon_\alpha = 1$ in the λ-region and $\varepsilon_\alpha = \varepsilon_{\alpha\pi}$ in the π-region; where:

$$\varepsilon_{\alpha\pi} = 1 - \frac{l_\sigma^2}{L^2}. \tag{10}$$

In order to derive the averaging governing equations, the spatial average theorem of a generic function Ψ_α is applied [14]:

$$\overline{\nabla \Psi_\alpha} = \nabla \overline{\Psi}_\alpha + \frac{1}{\mathcal{V}} \int_{S_{\alpha\sigma}} \mathbf{n}_{\alpha\sigma} \Psi_\alpha dS. \tag{11}$$

When this theorem is applied to a constant ψ_α we obtain:

$$\overline{\nabla \psi_\alpha} = -\frac{1}{\mathcal{V}} \int_{S_{\alpha\sigma}} \mathbf{n}_{\alpha\sigma} dS. \tag{12}$$

A. Continuity equation

The superficial volume average of the continuity Eq. (1) in $\mathcal{V}$

$$\overline{\nabla \cdot \mathbf{u}_\alpha} = 0 \tag{13}$$

is obtained by applying Eq. (11):

$$\nabla \cdot \bar{\mathbf{u}}_\alpha + \frac{1}{\mathcal{V}} \int_{S_{\alpha\sigma}} \mathbf{n}_{\alpha\sigma} \cdot \mathbf{u}_\alpha dS = 0; \tag{14}$$

and by imposing the boundary condition Eq. (3) at the α-σ–interface:

$$\nabla \cdot \bar{\mathbf{u}}_\alpha = 0 \tag{15}$$

B. Momentum equation

The superficial volume average is applied to Eq. (2):

$$0 = -\overline{\nabla p_\alpha} + \overline{\mu_\alpha \nabla^2 \mathbf{u}_\alpha} + \overline{\mathbf{f}_\alpha}. \tag{16}$$

Neglecting variations in ρ_α, μ_α and $\mathbf{f}_\alpha$, Eq. (16) reduces to:

$$0 = -\overline{\nabla p_\alpha} + \mu_\alpha \overline{\nabla^2 \mathbf{u}_\alpha} + \varepsilon_\alpha \mathbf{f}_\alpha. \tag{17}$$

Applying twice the superficial volume averaging Eq. (11) Eq. (17) we obtain:

$$\begin{aligned} 0 = & - \nabla \overline{p}_\alpha + \mu_\alpha \nabla^2 \overline{\mathbf{u}}_\alpha + \varepsilon_\alpha \mathbf{f}_\alpha \\ & + \frac{1}{\mathcal{V}} \int_{S_{\alpha\sigma}} \mathbf{n}_{\alpha\sigma} \cdot (-\mathbf{I} p_\alpha + \mu_\alpha \nabla \mathbf{u}_\alpha) dS. \end{aligned} \tag{18}$$

The superficial averaged velocity and the intrinsic averaged pressure are often preferred. The first because it is a hydrodynamic velocity directly related to the averaged volume and the latter due to the fact that this is the pressure that can be measure directly. We therefore recast Eq. (18) searching for preferred variables:

$$\begin{aligned} 0 = & - \varepsilon_\alpha \nabla \bar{p}_{\alpha,\bar{\alpha}} - \bar{p}_{\alpha,\bar{\alpha}} \nabla \varepsilon_\alpha + \mu_\alpha \nabla^2 \overline{\mathbf{u}}_\alpha + \varepsilon_\alpha \mathbf{f}_\alpha \\ & + \frac{1}{\mathcal{V}} \int_{S_{\alpha\sigma}} \mathbf{n}_{\alpha\sigma} \cdot (-\mathbf{I} p_\alpha + \mu \nabla \mathbf{u}_\alpha) dS. \end{aligned} \tag{19}$$

Using Eq. (12) in the right-hand side of Eq. (19) we interchange differentiation and integration for the second term:

$$\bar{p}_{\alpha,\bar{\alpha}}\nabla\varepsilon_\alpha = -\frac{1}{\mathcal{V}}\int_{S_{\alpha\sigma}} \mathbf{n}_{\alpha\sigma}\cdot\bar{p}_{\alpha,\bar{\alpha}}dS. \tag{20}$$

Additionally, to get the fluctuating stress tensor in the integral term ($\hat{\phi}_\alpha = \phi_\alpha - \bar{\phi}_{\alpha,\bar{\alpha}}$ being a fluctuating variable) we introduce the following terms by applying Eq. (12):

$$\nabla\varepsilon_\alpha\cdot\nabla\bar{\mathbf{u}}_{\alpha,\bar{\alpha}} + \frac{1}{\mathcal{V}}\int_{S_{\alpha\sigma}} \mathbf{n}_{\alpha\sigma}\cdot\nabla\bar{\mathbf{u}}_{\alpha,\bar{\alpha}}dS = 0. \tag{21}$$

Applying Eqs. (19), (20) and (21),and dividing by ε_α we obtain:

$$\begin{aligned} 0 \;&= -\nabla\bar{p}_{\alpha,\bar{\alpha}} + \frac{\mu_\alpha}{\varepsilon_\alpha}\nabla^2\bar{\mathbf{u}}_\alpha + \mathbf{f}_\alpha - \frac{\mu_\alpha}{\varepsilon_\alpha}\left(\nabla\varepsilon_\alpha\cdot\nabla\bar{\mathbf{u}}_{\alpha,\bar{\alpha}}\right) \\ &+ \frac{1}{\mathcal{V}}\int_{S_{\alpha\sigma}} \mathbf{n}_{\alpha\sigma}\cdot[-\mathbf{I}(p_\alpha - \bar{p}_{\alpha,\bar{\alpha}}) + \mu_\alpha(\nabla\mathbf{u}_\alpha - \nabla\bar{\mathbf{u}}_{\alpha,\bar{\alpha}})]dS. \end{aligned} \tag{22}$$

The last term is the fluctuating stress tensor

$$\begin{aligned} \mu_\alpha\mathbf{K}_\alpha^{-1}(\mathbf{x})\cdot\overline{\mathbf{u}}_\alpha \;&= \\ &- \frac{1}{\mathcal{V}}\int_{S_{\alpha\sigma}} \mathbf{n}_{\alpha\sigma}\cdot(-\mathbf{I}\hat{p}_\alpha + \mu_\alpha\nabla\hat{\mathbf{u}}_\alpha)dS; \end{aligned} \tag{23}$$

and it is equal to zero in the λ-region and equal to the permeability under some length conditions [42] in the homogeneous π-region. These conditions are:

$$\frac{L_x L_z}{L_\varepsilon L_{\nabla p}} \ll 1; \tag{24}$$

$$\frac{L_x L_z}{L_\varepsilon L_{\nabla^2 u}} \ll 1; \tag{25}$$

$$\frac{L_x - l_{\sigma x}}{L_x} \ll 1; \tag{26}$$

$$\frac{L_z - l_{\sigma z}}{L_z} \ll 1; \tag{27}$$

where L_ε, $L_{\nabla p}$ and $L_{\nabla^2 u}$ are characteristic lengths related to the spatial variation of the porosity, the pressure gradient and the viscous term, respectively. On the other hand, the fourth term in the right-hand side of Eq. (22) is the Brinkman correction.

III. POROUS LAYER MODEL

The averaged three-dimensional system of equations valid in the whole domain Eqs. (15) and (22) is now simplified considering one-dimensional flow and length constrains. Additionally, only one phase is considered and subscript α is neglected from here on. Therefore,

we obtain the reduced-order approach to be used for modeling rough microchannels:

$$\begin{aligned} 0 \;=\; & -\frac{d\bar{p}_{\bar{\alpha}}}{dx} + \frac{\mu}{\varepsilon(y)}\frac{d^2\bar{u}(y)}{dy^2} + f_x \\ & - \frac{\mu}{\varepsilon(y)}\frac{d\varepsilon(y)}{dy}\frac{d\bar{u}_{\bar{\alpha}}(y)}{dy} - \mu K^{-1}(y)\bar{u}(y). \end{aligned} \tag{28}$$

For expressing the previous equation in dimensionless form, and considering the characteristic length equal to H, the following non-dimensional variables are introduced:

$$\tilde{x} = \frac{x}{H}, \quad \tilde{y} = \frac{y}{H}, \quad \tilde{u} = \frac{\bar{u}}{u_0}; \tag{29}$$

where $u_0 = \dot{m}/(\rho H)$ is the average velocity, $\dot{m}$ being the mass flow rate. Additionaly, the following dimensionless numbers are defined using the hydraulic diameter of the channel $D_h = 2H$ as characteristic length:

$$f_D \;=\; \frac{\tau_w}{\frac{1}{2}\rho u_0} = \frac{-\frac{d\bar{p}_{\bar{\alpha}}}{dx}}{\frac{\rho u_0^2}{4H}}; \tag{30}$$

$$\mathrm{Re} \;=\; \frac{2\rho u_0 H}{\mu} = \frac{2\dot{m}}{\mu}; \tag{31}$$

$$\mathrm{Po} \;=\; f_D\mathrm{Re} = \frac{-\frac{d\bar{p}_{\bar{\alpha}}}{dx}}{\frac{\mu u_0}{8H^2}}; \tag{32}$$

$$\mathrm{Da} \;=\; \frac{K}{4H^2} = \frac{1}{4}\frac{K}{l_\sigma^2}\frac{l_\sigma^2}{H^2}; \tag{33}$$

$$\tilde{a}_x \;=\; \frac{f_x}{\frac{\rho u_0^2}{4H}}; \tag{34}$$

where f_D is the friction factor (ratio between wall shear stress tensor and dynamic pressure), Re is the Reynolds number (ratio between convective and viscous forces), Po is the Poiseuille number (the product of the two previous numbers), Da is the Darcy number (or the dimensionless permeability), and $\tilde{a}_x$ is an additional friction factor in the x-direction to account for other external body forces (*eg* gravity, which would lead to a term proportional to the inverse square Froude number Fr^{-2}). Notice that, due to the definition of different characteristic lengths for dimensionless coordinates and dimensionless numbers, we call f_D to the Darcy friction factor, which is actually four times the Fanning (or skin) friction factor f [20]. Notice also, that the characteristic length for the Darcy number is H in order to be consistent with the Darcy friction factor definition. Other dimensionless numbers can appear depending of the fluid flow considered. For instance, for the compressible Stokes equations,

the Mach number (Ma) defines the flow; or if a biphasic fluid is taken into account in a microchannel the capillary number (Ca) will be present in the equations.

Recasting Eq. (28) in a dimensionless form we obtain for the porous π–region:

$$0 = \frac{\mathrm{Po}}{8} + \frac{1}{\varepsilon}\frac{d^2\tilde{u}}{d\tilde{y}^2} + \frac{\mathrm{Re}\tilde{a}_x}{8} - \frac{1}{\varepsilon}\frac{d\varepsilon}{d\tilde{y}}\frac{d\tilde{u}_{\tilde{\alpha}}}{d\tilde{y}} - \frac{1}{4Da}\tilde{u}; \tag{35}$$

and for the λ–region:

$$0 = \frac{\mathrm{Po}}{8} + \frac{d^2\tilde{u}}{d\tilde{y}^2} + \frac{\mathrm{Re}\tilde{a}_x}{8}. \tag{36}$$

Equation (35) is actually valid in all the domain, as $\mathrm{Da}^{-1} \to 0$ and $\varepsilon \to 1$ and is constant in the λ–region.

A. Stress tensor in porous media

Previous one-dimensional layer approaches for describing the flow in rough microchannels [2, 10, 19, 20] use experimental or numerical data for computing the drag related to the fluctuating stress tensor, namely the permeability, assuming the length restrictions described above. In this work we preserve these length restrictions and we adopt a discrete-element approach [2, 10] initially proposed by Taylor et al. [34] for modeling rough walls in turbulent flows. In this approach [34], the flow in the layer below the roughness top was approximated by a series of two-dimensional wall-parallel slices, computing the drag in each of them using a turbulence model. Using this approach they succeed in estimate ab initio the drag characteristic of sparse roughness [30]. In this section, a 2D model for predicting the permeability of laminar flow through 2D isotropic homogeneous porous media will be discussed shortly in this section [43]. The pore-scale model, shown in Fig. 2(a), is based on a rectangular geometry and is referred to as the RUC-pore model, meaning Representative Unit Cell at the pore scale. The unit cell in the homogeneous porous region has a volume $\mathcal{V}_{h\pi}$ (see also Fig. 1), and the solid fiber with volume $V_{\sigma\pi}$ represents the average solid geometry of the porous medium. The porosity is defined as:

$$\varepsilon_{\alpha\pi} = \frac{V_{\alpha\pi}}{\mathcal{V}_{h\pi}}, \tag{37}$$

where $V_{\alpha\pi}$ denotes the total fluid volume of the pore-scale unit cell. For simplicity we will use thereafter ε to refer to the porosity in the porous region $\varepsilon_{\alpha\pi}$ and we consider that

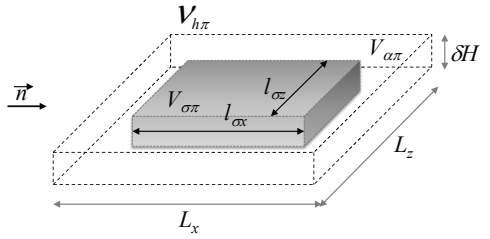

(a) Representative Unit Cell at the pore level (RUC-pore)

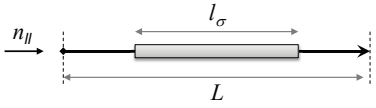

(b) Streamwise 1D reference domain

FIG. 2: Representative Unit Cell for fibre beds.

$l_{\sigma x} = l_{\sigma z} = l_\sigma$ and $L_x = L_z = L$. The relation between the linear dimensions, Fig. 2(b), is given by

$$l_\sigma = L(1-\varepsilon)^{1/2}. \tag{38}$$

A direct modeling procedure is followed in which piece-wise plane-Poiseuille flow is assumed in all channel sections. The relation between the streamwise and transverse wall shear stresses, denoted by $\tau_{w_\parallel}$ and $\tau_{w_\perp}$, respectively, may thus be expressed as

$$\tau_{w_\parallel} = \frac{6\mu\bar{u}_{\parallel\bar{\alpha}}}{L-l_\sigma} = \frac{1}{\beta\xi}\tau_{w_\perp}, \tag{39}$$

where $\bar{u}_{\parallel\bar{\alpha}}$ is the magnitude of the intrinsic streamwise average channel velocity. The coefficient β is defined as the ratio of the streamwise average channel velocity over the transverse average channel velocity. The coefficient ξ was introduced to account for the reduction in the tortuosity due to the splitting of the streamwise flux into two equal but directionally opposite transverse parts in a staggered array. Two arrays are considered, as shown in Fig. 3. In a regular array no staggering occurs and in a fully staggered array maximum possible staggering occurs in the streamwise direction, denoted by $\vec{n}$. For a regular array $\beta = \xi = 0$ and for a fully staggered array $\beta = \xi = 1/2$.

The total streamwise pressure drop over a unit cell of length L, denoted by δp, may be expressed as

$$\delta p = \frac{12(1+\beta\xi)\mu\bar{u}_{\parallel\bar{\alpha}}l_\sigma}{(L-l_\sigma)^2} = \frac{12(1+\beta\xi)\mu\bar{u}_{\parallel}l_\sigma L}{(L-l_\sigma)^3}, \tag{40}$$

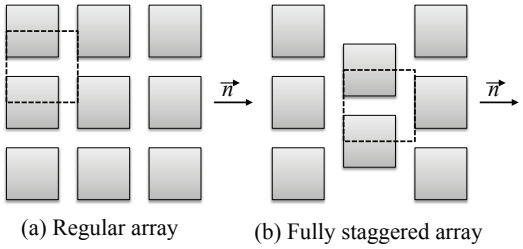

FIG. 3: A schematic representation of a regular and fully staggered array

where $\bar{u}_{\|}$ denotes the magnitude of the superficial velocity

$$\bar{u}_{\|} = \varepsilon_{\|}\bar{u}_{\|\bar{\alpha}} = [1-(1-\varepsilon)^{1/2}]\bar{u}_{\|\bar{\alpha}}. \tag{41}$$

The permeability K can there-upon be expressed as:

$$K = \frac{\mu\bar{u}_{\|}}{\delta p/L} = \frac{(L-l_\sigma)^3}{12(1+\beta\xi)l_\sigma}. \tag{42}$$

Using Eq. (38) we can write a dimensionless permeability based on the characteristic length l_σ:

$$\frac{K}{l_\sigma^2} = \frac{(1-\sqrt{1-\varepsilon})^3}{12(1+\beta\xi)(1-\varepsilon)^{3/2}}. \tag{43}$$

A 2D isotropic homogeneous porous model is obtained by taking the average of the coefficients of a regular and a fully staggered array, thus yielding

$$\frac{K}{l_\sigma^2} = \frac{(1-\sqrt{1-\varepsilon})^3}{(27/2)(1-\varepsilon)^{3/2}}. \tag{44}$$

The advantage of the RUC-pore model is that it is based on sound physical principles and therefore contains no empirical coefficients.

We compare now several numerical and experimental expression used to define the permeability in porous media, see Table II, with the result obtained in Eq. (44). The comparison is shown in Fig. 4.

IV. ONE-REGION POROUS-LAYER MODEL

Let us consider a channel like in Fig. 1(a), where H represent half of the total height. As the PLM Eq. (28) is valid for both π- and λ-regions, we can solve this equation in the whole domain to obtain the velocity profiles. In order this equation to be differentiable in

Author	Geometry	K/l_σ^2	Origin
Carman-Kozeny (1956) [4]	3D - isotropic	$\frac{\varepsilon^3}{150(1-\varepsilon)^2}$	Fitting experimental data
Kaviany (1999) [17]	3D - isotropic	$\frac{0.002\varepsilon^3}{(1-\varepsilon)^{8/3}}$	Fitting experimental data
Du Plessis (2008) [8]	3D - isotropic	$\frac{[1-(1-\varepsilon)^{1/3}][1-(1-\varepsilon)^{2/3}]^2}{25.4(1-\varepsilon)^{4/3}}$	Simple pore model
Gamrat *et al.*(2008) [10]	2D - aligned	$\frac{2(1-\varepsilon)^{-1}}{52.2(1-\varepsilon)^{0.27}e^{4.5(1-\varepsilon)}}$	2D CFD simulations
Gamrat *et al.*(2008) [10]	2D - staggered	$\frac{2(1-\varepsilon)^{-1}}{62.2(1-\varepsilon)^{0.28}e^{4.64(1-\varepsilon)}}$	2D CFD simulations
Woudberg (2009) [43]	2D - isotropic	$\frac{(1-\sqrt{1-\varepsilon})^3}{(27/2)(1-\varepsilon)^{3/2}}$	Simple pore model

TABLE II: Expressions for the dimensionless permeability K/l_σ, where K is the permeability and l_σ is the characteristic length of the unit solid obstacle.

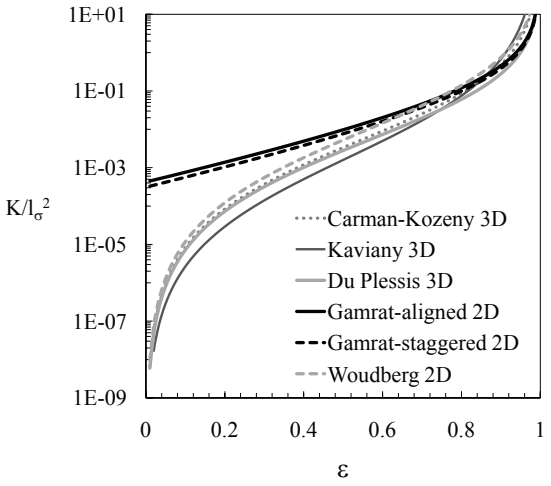

FIG. 4: Dimensionless permeability K/l_σ versus the porosity ε for expression in Table II.

the whole range of y, a function for the smooth variation of the porosity must be provided. Considering the periodically distributed parallelepiped elements described in Fig 1(c), we define the smooth spatial variation of $l_\sigma = l_{\sigma x} = l_{\sigma z}$ according to the function:

$$l_\sigma(y) = \zeta(y) l_{\sigma 0}; \tag{45}$$

where $\zeta(y)$ is and smooth logistic function, which define the evolution of geometric properties without discontinuities within the whole domain:

$$\zeta(y) = \frac{1 + \frac{y}{k}(\varphi - 1)}{1 + \exp(\frac{y-k}{\epsilon})}; \tag{46}$$

$$l_\sigma(0) = l_{\sigma 0}; \tag{47}$$

$$\varphi = \frac{l_\sigma(k)}{l_\sigma(0)}; \tag{48}$$

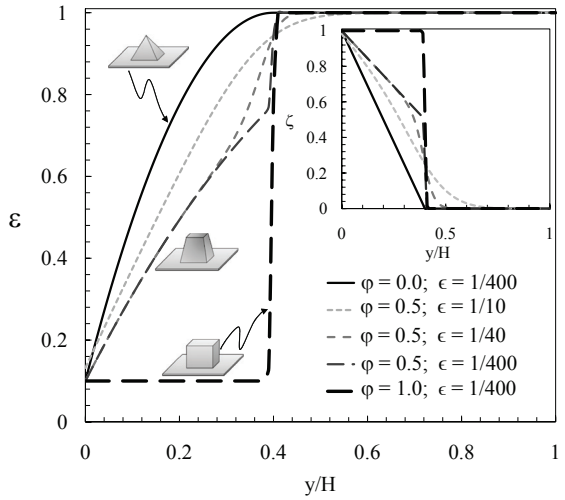

FIG. 5: Porosity ε, taken $k = 0.4$ and $H = 1$, as a function of y for $\varphi = 0$ (pyramids), $\varphi = 1/2$ (truncated pyramids) and $\varphi = 1$ (cubes). For truncated pyramids three values of ϵ are showed to illustrate its influence; otherwise $\epsilon = 1/400$. In the inset, the smooth geometric function $\zeta(y)$, Eq. (46), is depicted.

and ϵ being a small parameter to control the slope of the transition. An expression for the porosity is obtained using Eqs. (10) and (45):

$$\varepsilon(y) = 1 - \zeta^2(y)\frac{l_{\sigma 0}^2}{L^2}. \tag{49}$$

Plotting this expression for several values of φ, Fig. 5 we recover the evolution of the porosity along y for different geometries of the rough structure. This plot also shows the spatial evolution of ζ.

The study of the existence of analytical solutions [1, 23, 28, 45] for Eq. (28) reveals that it only exists if the porosity is constant through the domain (there exists another particular analytical solution with no physical interest for the case when $K^{-1}(y) = \varepsilon^{-3}(y)[d_y\varepsilon(y)]^2$). Therefore, as we are not interested in the case of a channel with constant porosity, when the one-region approach is selected we must use numerical approximations to find the solution. For numerical convenience (lower computational cost), the logistic approach for defining the variation of properties can be expressed alternatively by an algebraic expression:

$$\begin{aligned}\zeta(y) \;&=\; \frac{1}{2k\kappa}[k(k+\kappa) \\ &+\; [\Upsilon(\varphi-1) + k(\varphi-2)]\, y + (1-\varphi)y^2];\end{aligned} \tag{50}$$

where

$$\kappa = \epsilon \left[1 + \frac{(k-y)^2}{\epsilon^2} \right]^{1/2}. \tag{51}$$

However, the low computational demand of the numerical approach should not be the limiting step; unless the subroutine was extensively use in lump simulation of a more complex system, where moving to Eq. (50) would have sense.

V. TWO-REGION POROUS-LAYER MODEL

An alternative approach, which should be completely equivalent, is to split the domain in two numerical domains corresponding to the physical regions. For the porous π–region we solve Eq. (35) and for the fluid one Eq. (36). These two domains are coupled through appropriate boundary conditions. In the following, we analyzed which are the proper boundary conditions to couple these equations, and we also describe the existing analytical solutions.

A. Generalized inter-region boundary condition

The derivation of the boundary conditions sketched here follows previous works [26, 38] about jump conditions between porous and fluid mediums. For deriving the boundary jump condition, a integration volume $\mathcal{V}_I$ as the one depicted in Fig. 1(c) is used. This volume can be decomposed as:

$$\mathcal{V}_I = V_{\alpha\lambda} + V_{\alpha\pi} + V_{\sigma\pi} = \mathcal{V}_\lambda + \mathcal{V}_\pi; \tag{52}$$

and the area S_I surrounding $\mathcal{V}_I$ can be represented in terms of the bounding surfaces in the λ- and π- regions according to

$$S_I = S_\lambda + S_\pi. \tag{53}$$

The system of equations to be solved for the porous region $\mathcal{V}_\pi$ within $\mathcal{V}_I$ is:

$$\nabla \cdot \bar{\mathbf{u}}_\pi(y) = 0; \tag{54}$$

$$\begin{aligned} 0 &= -\nabla \bar{p}_{\pi,\bar{\alpha}} + \frac{\mu}{\varepsilon} \nabla^2 \bar{\mathbf{u}}_\pi \\ &- \mu \mathbf{K}_\pi^{-1} \cdot \overline{\mathbf{u}}_\pi; \end{aligned} \tag{55}$$

and for the liquid region:

$$\nabla \cdot \bar{\mathbf{u}}_\lambda(y) \;=\; 0; \tag{56}$$

$$0 \;=\; -\nabla \bar{p}_{\lambda,\bar{\alpha}} + \frac{\mu}{\varepsilon}\nabla^2 \bar{\mathbf{u}}_\lambda; \tag{57}$$

where subcripts λ and π are use to denote the pressure and velocity in the α–phase of the liquid and porous region respectively.

1. *Continuity equation*

Integrating Eq. (1) we obtain:

$$\int_{\mathcal{V}_I} \nabla \cdot \bar{\mathbf{u}} dV = 0; \tag{58}$$

and applying the divergence theorem

$$0 = \int_{S_I} \mathbf{n} \cdot \bar{\mathbf{u}} dS = \int_{S_\lambda} \mathbf{n}_\lambda \cdot \bar{\mathbf{u}} dS + \int_{S_\pi} \mathbf{n}_\pi \cdot \bar{\mathbf{u}} dS. \tag{59}$$

In the same way, performing this integration on Eq. (54) and (56) leads to

$$\int_{S_\pi} \mathbf{n}_\pi \cdot \bar{\mathbf{u}}_\pi dS + \int_{S_{\pi\lambda}} \mathbf{n}_{\pi\lambda} \cdot \bar{\mathbf{u}}_\pi dS \;=\; 0; \tag{60}$$

$$\int_{S_\lambda} \mathbf{n}_\lambda \cdot \bar{\mathbf{u}}_\lambda dS + \int_{S_{\lambda\pi}} \mathbf{n}_{\lambda\pi} \cdot \bar{\mathbf{u}}_\lambda dS \;=\; 0; \tag{61}$$

where $S_{\pi\lambda} = S_{\lambda\pi}$ represent the area of the interface contained in $\mathcal{V}_I$, and $\mathbf{n}_{\lambda\pi} = -\mathbf{n}_{\pi\lambda}$ the normal vector. Subtracting Eq. (60) and (61) from Eq. (59) and rearranging the result we have

$$\begin{aligned} \int_{S_{\pi\lambda}} \mathbf{n}_{\pi\lambda} \cdot \Big(\bar{\mathbf{u}}_\pi - \bar{\mathbf{u}}_\lambda\Big) dS \;=\; & \int_{S_\pi} \mathbf{n}_\pi \cdot \Big(\bar{\mathbf{u}} - \bar{\mathbf{u}}_\pi\Big) dS \\ & + \int_{S_\lambda} \mathbf{n}_\lambda \cdot \Big(\bar{\mathbf{u}} - \bar{\mathbf{u}}_\lambda\Big) dS. \end{aligned} \tag{62}$$

The excess surface velocity is defined as [26]

$$\begin{aligned} \oint_C \mathbf{n}_s \cdot \Big(\delta \bar{\mathbf{u}}_s\Big) d\sigma \;=\; & \int_{S_\pi} \mathbf{n}_\pi \cdot \Big(\bar{\mathbf{u}} - \bar{\mathbf{u}}_\pi\Big) \\ & + \int_{S_\lambda} \mathbf{n}_\lambda \cdot \Big(\bar{\mathbf{u}} - \bar{\mathbf{u}}_\lambda\Big); \end{aligned} \tag{63}$$

where C is a closed curved lying on the dividing surface. Using Eq. (63)with Eq. (62) and applying the Stokes theorem leads to

$$\mathbf{n}_{\pi\lambda} \cdot \Big(\bar{\mathbf{u}}_\pi - \bar{\mathbf{u}}_\lambda\Big) = \nabla_s \cdot \Big(\delta \bar{\mathbf{u}}_s\Big). \tag{64}$$

Usually, the effect of the excess surface velocity can be neglected in a homogeneous porous-fluid interface, leading to the boundary conditions for velocities

$$\mathbf{n}_{\pi\lambda} \cdot \Big(\bar{\mathbf{u}}_\pi - \bar{\mathbf{u}}_\lambda\Big) = 0. \tag{65}$$

2. Momentum equation

To derive the momentum jump condition, is convenient to first rewrite Eq. (28) in the form

$$\begin{aligned} 0 \;=\; & -\nabla \bar{p}_{\bar{\alpha}} + \mu \nabla \cdot \Big(\varepsilon^{-1} \nabla \bar{\mathbf{u}}\Big) \\ & -\; \mu \varepsilon^{-3} (\nabla \varepsilon \cdot \nabla \varepsilon) \bar{\mathbf{u}} - \mu \mathbf{K}^{-1} \cdot \bar{\mathbf{u}}. \end{aligned} \tag{66}$$

Integrating Eqs. (66), (55) and (57) as for the continuity equation, we obtain:

$$\begin{aligned} \int_{S_{\pi\lambda}} \mathbf{n}_{\pi\lambda} \;\cdot\; & [-\mathbf{I}(\bar{p}_{\pi,\bar{\alpha}} - \bar{p}_{\lambda,\bar{\alpha}}) + \mu(\varepsilon_\pi^{-1} \nabla \bar{\mathbf{u}}_\pi - \nabla \bar{\mathbf{u}}_\lambda)] dS \\ = & -\int_{S_\pi} \mathbf{n}_\pi \cdot \Big(\bar{p}_{\bar{\alpha}} - \bar{p}_{\pi,\bar{\alpha}}\Big) dS \\ & -\int_{S_\lambda} \mathbf{n}_\lambda \cdot \Big(\bar{p}_{\bar{\alpha}} - \bar{p}_{\lambda,\bar{\alpha}}\Big) dS \\ & +\int_{S_\pi} \mu \mathbf{n}_\pi \cdot \Big(\varepsilon^{-1} \nabla \bar{\mathbf{u}} - \varepsilon_\pi^{-1} \nabla \bar{\mathbf{u}}_\pi\Big) dS \\ & +\int_{S_\lambda} \mu \mathbf{n}_\lambda \cdot \Big(\varepsilon^{-1} \nabla \bar{\mathbf{u}} - \nabla \bar{\mathbf{u}}_\lambda\Big) dS \\ & +\int_{\mathcal{V}_I} \mu \varepsilon^{-3} (\nabla \varepsilon \cdot \nabla \varepsilon) \bar{\mathbf{u}} dV \\ & -\int_{\mathcal{V}_I} \mu \mathbf{K}^{-1} \cdot \bar{\mathbf{u}} dV \\ & +\int_{\mathcal{V}_\pi} \mu \mathbf{K}_\pi^{-1} \cdot \bar{\mathbf{u}}_\pi dV; \end{aligned} \tag{67}$$

where ε_π is a constant value describing the homogeneous porosity in the porous media close to the interface. The following terms are defined [26]: (i) the excess surface stress

$$\begin{aligned}\oint_C \mathbf{n}_s \cdot (\delta\bar{\mathbf{T}}_s)d\sigma &= \int_{S_\pi} \mathbf{n}_\pi \cdot [-\mathbf{I}(\bar{p}_{\bar{\alpha}} - \bar{p}_{\pi,\bar{\alpha}}) \\ &+ \mu(\varepsilon^{-1}\nabla\bar{\mathbf{u}} - \varepsilon_\pi^{-1}\nabla\bar{\mathbf{u}}_\pi)]dS \\ &+ \int_{S_\lambda} \mathbf{n}_\lambda \cdot [-\mathbf{I}(\bar{p}_{\bar{\alpha}} - \bar{p}_{\lambda,\bar{\alpha}}) \\ &+ \mu(\varepsilon^{-1}\nabla\bar{\mathbf{u}} - \nabla\bar{\mathbf{u}}_\lambda)]dS; \end{aligned} \tag{68}$$

(ii) the excess Brinkman stress

$$\int_{S_{\pi\lambda}} \mathbf{n}_{\pi\lambda} \cdot \bar{\mathbf{B}}_s dS = \int_{\mathcal{V}_I} \mu_\alpha \varepsilon^{-3}(\nabla\varepsilon \cdot \nabla\varepsilon)\bar{\mathbf{u}}dV. \tag{69}$$

and (iii) the excess bulk stress

$$\int_{S_{\pi\lambda}} \mathbf{n}_{\pi\lambda} \cdot \bar{\mathbf{T}}_s dS = \int_{\mathcal{V}_I} \mu\mathbf{K}^{-1} \cdot \bar{\mathbf{u}}dV - \int_{\mathcal{V}_\pi} \mu\mathbf{K}_\pi^{-1} \cdot \bar{\mathbf{u}}_\pi dV; \tag{70}$$

Additionally, the following equivalences are considered [38]:

$$\int_{S_{\pi\lambda}} \mathbf{n}_{\pi\lambda} \cdot \bar{\mathbf{B}}_s dS = \left[\frac{\mu}{a_{vs}}\varepsilon^{-3}(\nabla\varepsilon \cdot \nabla\varepsilon)\bar{\mathbf{u}}\right]_{\pi\lambda}; \tag{71}$$

$$\int_{S_{\pi\lambda}} \mathbf{n}_{\pi\lambda} \cdot \bar{\mathbf{T}}_s dS = -\left[\frac{\mu}{a_{vs}}\mathbf{K}^{-1} \cdot \bar{\mathbf{u}}\right]_{\pi\lambda}; \tag{72}$$

where a_{vs} is ratio between the fluid-solid $\alpha\sigma$–interphase $S_{\pi\lambda}$ and the total volume $\mathcal{V}_\pi$.

Introducing Eqs. (68-72) in Eq. (67) we obtain:

$$\begin{aligned} &-\mathbf{n}_{\pi\lambda} \cdot (\bar{p}_{\pi,\bar{\alpha}} - \bar{p}_{\lambda,\bar{\alpha}}) + \mu\mathbf{n}_{\pi\lambda} \cdot (\varepsilon_\pi^{-1}\nabla\bar{\mathbf{u}}_\pi - \nabla\bar{\mathbf{u}}_\lambda) \\ &= \nabla_s \cdot \delta\bar{T}_s + \left[\frac{\mu}{a_{vs}}\mathbf{K}^{-1} \cdot \bar{\mathbf{u}}\right]_{\pi\lambda} \\ &+ \left[\frac{\mu}{a_{vs}}\varepsilon^{-3}(\nabla\varepsilon \cdot \nabla\varepsilon)\bar{\mathbf{u}}\right]_{\pi\lambda}; \end{aligned} \tag{73}$$

where the first term in the right-hand-side is the surface stress, the sencond one is the global stress and the third term is the Brinkman stress. The surface stress can be assumed to be negligible for a porous-fluid interface [26] and the contribution of Brinkman stress is negligible [38]. Therefore, from Eq. (73) we can extract the following two boundary conditions at the interface, one for the pressure:

$$-\mathbf{n}_{\pi\lambda}(\bar{p}_{\pi,\bar{\alpha}} - \bar{p}_{\lambda,\bar{\alpha}}) = 0; \tag{74}$$

and other for the jump of the stress:

$$\mathbf{n}_{\pi\lambda} \cdot (\varepsilon_{\alpha\pi}^{-1}\nabla\bar{\mathbf{u}}_\pi - \nabla\bar{\mathbf{u}}_\lambda) = -\frac{\mathbf{K}_\alpha^{-1}}{a_{vs}} \cdot \bar{\mathbf{u}}_\pi. \tag{75}$$

B. Analytical solutions

As for the one-region approach, there only exists analytical solutions [1, 23, 28, 45] for the case of constant porosity ε. However, due to the splitting in two numerical domains, the two-regions approach has analytical solution for some case of interest. Specifically, a rough channel with the following boundary conditions is solved:

$$\begin{aligned} \tilde{u}_\pi(0) &= 0; \\ \tilde{u}_\lambda(k) &= \tilde{u}_\pi(k); \\ \frac{d\tilde{u}_\lambda}{d\tilde{y}}(1) &= 0; \\ \varepsilon^{-1}\frac{d\tilde{u}_\pi(\tilde{k})}{d\tilde{y}} - \frac{d\tilde{u}_\lambda(k)}{d\tilde{y}} &= -\tilde{J}\tilde{u}_\pi(\tilde{k}); \end{aligned} \tag{76}$$

where:

$$\tilde{J} = (HK_s^{-1})/(a_{\mathrm{vs}}) \tag{77}$$

is the dimensionless stress jump coefficient.

The analytical solution obtained is:

$$\begin{aligned} \tilde{u}_\pi &= \left[4\left(2\sqrt{\mathrm{Da}}J\sqrt{\varepsilon}\sinh\left(A_k\right) + \cosh\left(A_k\right)\right)\right]^{-1} \\ &\times \left[4\mathrm{DaPo}\sinh\left(A_y\right)\left(2\sqrt{\mathrm{Da}}J\sqrt{\varepsilon}\cosh\left(A_k - A_y\right) + \sinh\left(A_k - A_y\right)\right)\right. \\ &- \left.\sqrt{\mathrm{Da}}\mathrm{Po}\sqrt{\varepsilon}(4\mathrm{Da}J + \tilde{k} - 1)\sinh\left(2A_y\right)\right]; \end{aligned} \tag{78}$$

$$\tilde{u}_\lambda = \mathrm{Po}\left[16\left(\left(2\sqrt{\mathrm{Da}}J\sqrt{\varepsilon}+1\right)\exp(2A_k) - 2\sqrt{\mathrm{Da}}J\sqrt{\varepsilon}+1\right)\right]^{-1}$$

(80)

$$\begin{aligned} &\times \left[2\sqrt{\mathrm{Da}}\sqrt{\varepsilon}\left(\exp(2A_k)-1\right)\left(J\tilde{k}^2 - 2(J+1)\tilde{k} - J(\tilde{y}-2)\tilde{y} + 2\right)\right. \\ &+ \left.(\tilde{k}-\tilde{y})(\tilde{k}+\tilde{y}-2)\left(\exp(2A_k)+1\right) + 8\mathrm{Da}\left(\exp(A_k)-1\right)^2\right]; \end{aligned} \tag{81}$$

where $A_y = (\tilde{y}\sqrt{\varepsilon})/(4\sqrt{\mathrm{Da}})$ and $A_k = (\tilde{k}\sqrt{\varepsilon})/(2\sqrt{\mathrm{Da}})$.

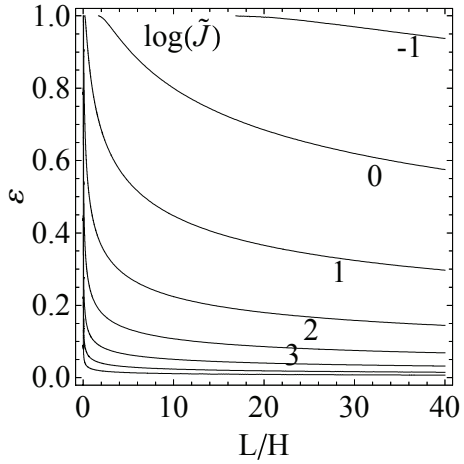

FIG. 6: Isocontours of $\log(\tilde{J})$ as a function of the relative length L/H and the porosity ε

The Po can be computed as a function of $\dot{m}$ by integrating the velocity profile:

$$\begin{aligned}
\mathrm{Po} \;=\; & \left[24\dot{m}\left(\left(2\sqrt{\mathrm{Da}}J\sqrt{\varepsilon}+1\right)\exp((2A_k)-2\sqrt{\mathrm{Da}}J\sqrt{\varepsilon}+1\right)\right] \\
\times\; & \rho^{-1}\Big[\frac{24\mathrm{Da}^{3/2}\left(\exp((2A_k)-1\right)\left(J\tilde{k}\varepsilon-1\right)}{\sqrt{\varepsilon}}-96\mathrm{Da}^2J\left(\exp(A_k)-1\right)^2 \\
-\; & 2\sqrt{\mathrm{Da}}(\tilde{k}-1)^2\sqrt{\varepsilon}(J(\tilde{k}-1)-3)\left(\exp(2A_k)-1\right)+(\tilde{k}-1)^3\left(-\left(\exp(2A_k)+1\right)\right) \\
+\; & 12\mathrm{Da}\left((2-\tilde{k})\exp(2A_k)+4(\tilde{k}-1)\exp(A_k)-\tilde{k}+2\right)\Big]^{-1}
\end{aligned} \tag{82}$$

Using the analytical solution for this rough channel we can study the influence of the roughness geometry in the jump coefficient, Fig. 6. It can be seen that the stress jump is greater for smaller porosities ε and relative lengths L/H of the domain.

VI. RESULTS

The Porous Layer Model presented is validated against CFD results of three geometries: (i) a rough channel with homogeneous parallelepiped roughness; (ii) a semi-rough channel with heterogeneous pyramid distribution; and (iii) a semi-rough channel with wavy surface. For all CFD simulations the geometry has been meshed in Gambit and solved with Fluent 6.3.26 using a SIMPLE algorithm. Convergence and grid independence of the solution was carefully verified. For those geometries with non-constant porosity within the porous region, data were extracted from the CFD models and interpolated via cubic polynomials to obtain the porosity across the whole domain; and a first order derivative scheme is used

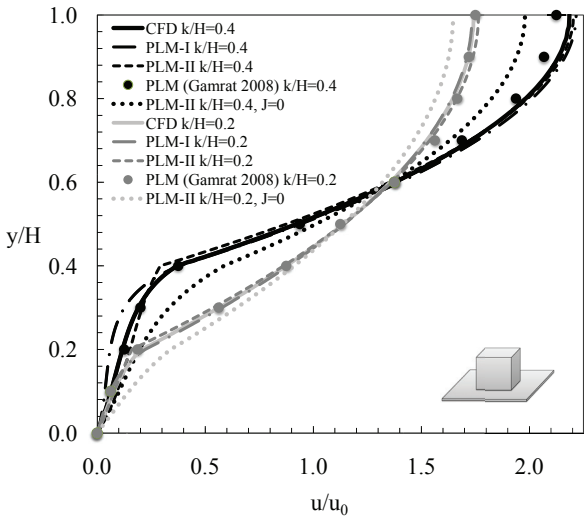

FIG. 7: Dimensionless velocity profile.

to obtain the porosity variation with height.

A numerical one-region approach (PLM-I) is applied to study a rough microchannel with periodically distributed parallelepiped elements, as the ones analyzed in Gamrat et al. [10], the porosity being constant through the rough layer. To avoid discontinuities across the domain, the porosity is defined by means of Eqs. (45) and (46). To compare the results, symmetry condition has been set at the top of the channel and dimensionless lengths have been used . Figures 7 and 8 show the good agreement between the CFD results and the PLM-I. Additional PLM results by Gamrat et al. [10] and an analytical two-region approach (PLM-II) are also plotted. Velocity profiles with a stress jump coefficient $J = 0$ show the solution behavior when no stress jump is considered. The latter remarks the importance of the jump stress in modeling rough microchannels.

The PLM-I was also applied to pyramidal semi-rough channels, as the ones in Valdés et al. [37]. In these channels one wall is assumed to be smooth while pyramidal elements are randomly distributed on the other one. The height of the peaks in not uniform and therefore the relative roughness is defined in terms of the maximum roughness height. The fluid area at different heights is extracted from the CFD models and interpolated via cubic polynomials. Table III shows the relevant geometric parameters of the models selected to validate the PLM-I. The original nomenclature [37] has been kept for clarity. The PML-I predictions, Figs. 9 and 10, compare well with the CFD results for relative roughness

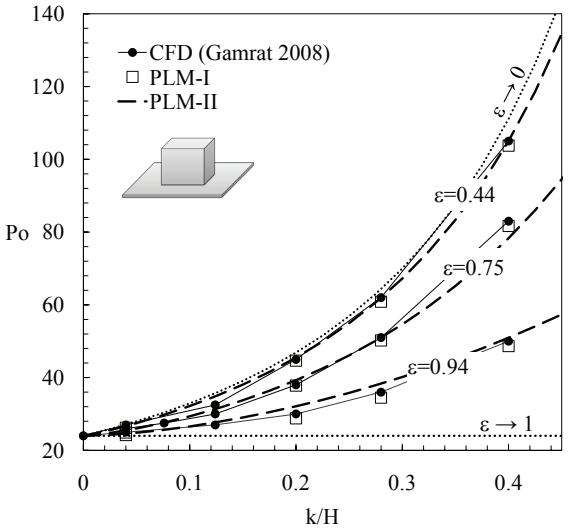

FIG. 8: Dimensionless pressure gradient Po versus the relative roughness k/H.

values well below unity. For high relative roughness channels the model underestimates the Poiseuille number.

Model	Averaged ε	#pyramids/m^2
M3	0.98	$3.3 \cdot 10^{10}$
M4	0.96	$6.0 \cdot 10^{10}$
M5	0.92	$1.2 \cdot 10^{11}$
M6	0.86	$6.0 \cdot 10^{10}$

TABLE III: Characteristics of the semi-rough channels with pyramidal rough elements.

Finally the PLM is used to predict the flow through channel with self-affine-like roughness. This roughness is generated by means of a 2D extension of the Weierstrass-Mandelbrot function:

$$h(x,y) = G^{D-1} \sum_{m=0}^{n} \gamma^{(D-2)m} \Big[\cos(2\pi\gamma^m x) + \cos(2\pi\gamma^m y) \Big];$$

where G is a scaling factor, D is the fractal parameter, γ is the fractal exponent, and n is the number of term in the series. This function is used only with $n = 0$ and $n = 1$, so modeled surfaces are wavy ones with no relevant self-affine property. Thus, the effect of self-affine variables is not studied. Results for the dimensionless pressure gradient are plotted in Fig. 11.

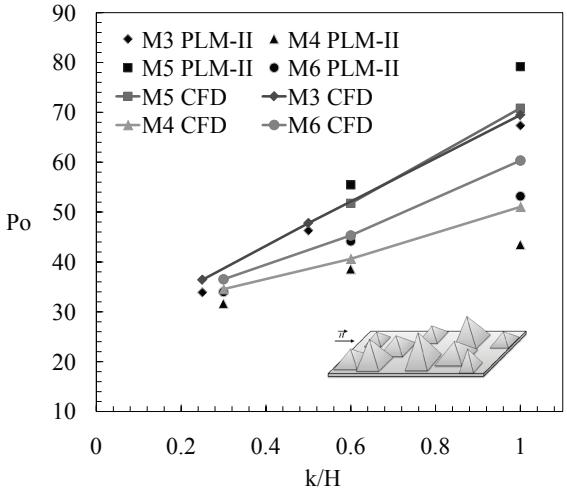

FIG. 9: Dimensionless pressure gradient Po versus the relative roughness k/H.

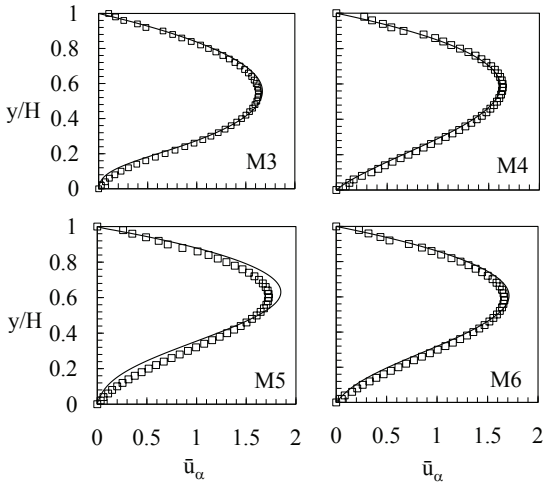

FIG. 10: Velocity profiles for M3 ($k/H = 0.3$), M4 ($k/H = 1$), M5 ($k/H = 0.6$), and M6 ($k/H = 0.6$), see Table III. Results are from averaged CFD (squares) and PLM-I (solid lines).

To summarize the results obtained we plot in Fig. 12 the relative error of Po for the three geometries. The linear fitting help us to approximate the applicability limits of the PLM (error below 10%): relative roughness $k/H < 0.5$, relative width $L/H < 30$ and porosity $\varepsilon < 0.8$.

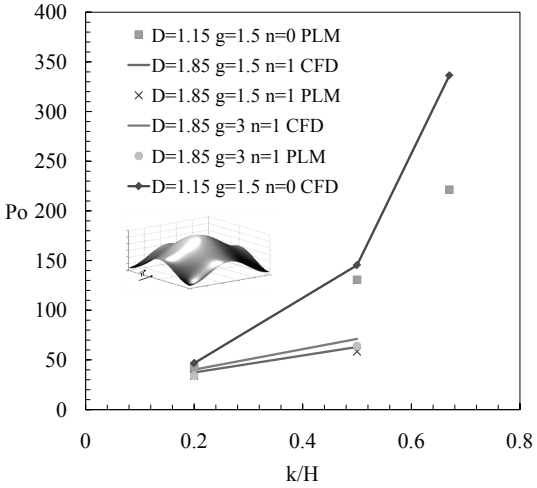

FIG. 11: Dimensionless pressure gradient Po versus the relative roughness k/H for three wavy surfaces defined by Eq. 83.

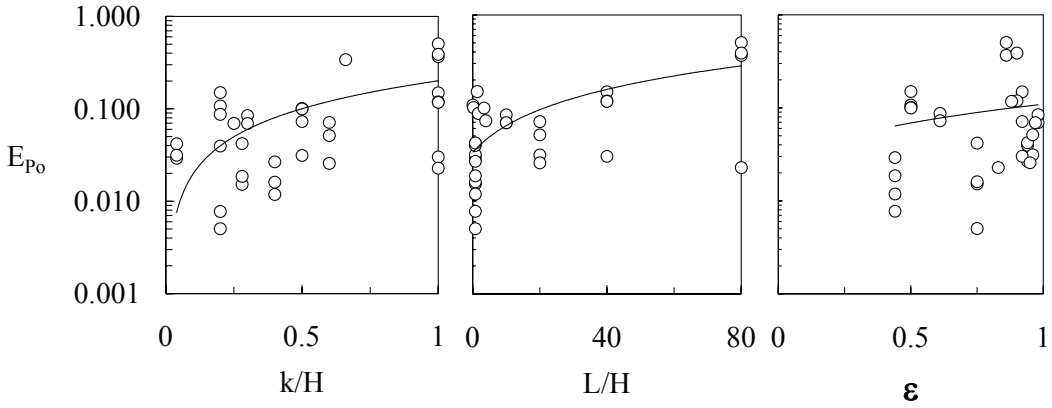

FIG. 12: Relative error Abs[Po(CFD)-Po(PLM)]/Po(CFD) versus relative roughness k/H (left); relative width L/H (center); and porosity ε (right). A linear fitting to the data is shown to guide the eye.

VII. CONCLUSIONS

A rigorous derivation of a Porous Layer Model (PLM) has been introduced as a reduced-order method to represent the fluid flow in rough microchannels. The novel results presented with regard to previous layer models are: the use of superficial average theorems to derive the one-dimensional average equations in rough microchannels; the derivation of the 2D permeability tensor from a simple porous unit cell model; the description of

one-region and two-region approaches for solving PLM, including the analysis of available analytical solutions; the compilation of assumption considered for developing the model (see the discussion below); and the derivation, using superficial average theorems, of the inter-region boundary condition for the two-region model. The most relevant consequence of this approach is that the model only uses the geometric characteristic of the surface as input parameters. Thus, it is not necessary additional experimental or numerical information about, for example, the structure of the stress tensor in the porous media as a function of the porosity. Velocity profiles and Pouseuille numbers has been compared for channels with different rough structures using solutions from CFD simulations and the one- and the two-region approaches. Results suggest that the model can be used for any kind of fluid-connected roughness structure for relative roughness $k/H < 0.5$, relative width $L/H < 30$ and porosity $\varepsilon < 0.8$ (if errors $< 10\%$ are assumed).

For the derivation of the PLM Eq. (28) several assumptions have been considered. These are: steady state; incompressibility (Ma$\to$0); single-component and single-phase with constant values for ρ_α, ν_α and f_α; continuous fluids (Kn$\to$0) in the very low Reynolds number limit (Re$\to$0) or Stokes regime, and without any special surface treatment; length several length assumptions have been considered, Eqs. (24–27) for obtaining an stress tensor equal to Darcy's permeability. Additionally, the discrete element approach by Taylor has been applied to simplify the treatment of the rough layer; thus, only fluid-connected rough surfaces can be modeled (see Sec. I). However, possible alternatives are available for the correction of these departures from the ideal properties discussed in Sec. I.

For example, Stokes equations are considered as the starting point. However, the inertial terms ($\rho\mathbf{u}\cdot\nabla\mathbf{u}$) cannot be negligible in boundary regions and should be introduced [3]. For departures from $(L - l_\sigma)/L \ll 1$ the effects in momentum loss due to recirculations should be taken into account [24]. For including surface effects the non-slip boundary condition at the interface α-σ can be applied [39]. If non-isotropic porous media are needed to be considered the approach proposed can be also applied [3]. Other aspect not considered in PLM is a possible mass source term [3]. This could be useful, for example, for modeling the wear of the surface due to mechanical or chemical mechanisms.

The method proposed is valid in the continuous limit. For low pressure gas flows the Stokes equations are no longer valid. Alternatively, two groups of approaches can be used,

after surface averaging of its corresponding macroscopic equation, to simulate rarified gases in rough channels. The first approach is based on modified Navier-Stokes equations, as, for example, the addition of terms for molecular diffusivity [7]; on the other hand, we could use de some moment system of equations with an appropriate closure, as the Grad's one [33]. Notice that this second approach could be used also for modeling polydispersive flows, such as granular or biphasic (bubbly) ones.

Summarizing the discussion, the averaging surface in conjunction with the simplified pore description, although it simplicity, leads to simple PLM with only geometric input parameters. Additionally, this approach can be further extended by including more physical phenomena without losing the simplicity. Thus, there exists a great potential in developing and using PLM's for its use in lump simulations of microfluidic applications.

The on-going work is devoted to the application of PLM for hydrodynamic-lubrication lump simulations by including into the model the effects of temporal and convective terms. The most challenging aspect is that for hydrodynamic-lubrication configurations we need to provide a solution for the permeability stress tensor without considering length restrictions Eqs. (24–27).

Acknowledgements

This work was partially funded by the FP6 EU KRISTAL project (Network of Excellence; Ref. 515837) and by the Spanish Government under project LUBRITECH, DPI2008-0648. SI acknowledges the support by the Spanish Government through its postdoctoral mobility fellowship programme. MA is supported by the Master Thesis ITA programme co-funded by the European Social Fund.

---

[1] M. Abramowitz and I. A. Stegun. *Handbook of mathematical functions: with formulas, graphs, and mathematical tables*. Courier Dover Publications, 1965.

[2] R. Bavière, G. Gamrat, M. Favre-Marinet, and S. Le Person. Modeling of laminar flows in rough-wall microchannels. *J. Fluids Eng.*, 128(4):734–741, 2006.

[3] P. Bousquet-Melou, B. Goyeau, M. Quintard, F. Fichot, and D. Gobin. Average momentum equation for the interdendritic flow in a solidifying columnar mushy zone. *Int. J. Heat Fluid*

Flow, 45:3651–3665, 2002.

[4] P. C. Carman. *Flow of Gases Through Porous Media*. Butterworths Scientific Publications, 1956.

[5] S. Chakraborty, T. Das, and S. Chattoraj. A generalized model for probing frictional characteristics of pressure-driven liquid microflows. *J. Appl. Phys.*, 102(10):104907, 2007.

[6] F. C. Colebrook. Turbulent flow in pipes, with particular reference to the transition region between the smooth and rough pipe laws. *J. Inst. Civ. Eng. London*, 11:133–156, 1939.

[7] N. Dongari, A. Sharma, and F. Durst. Pressure-driven diffusive gas flows in micro-channels: from the Knudsen to the continuum regimes. *Microfluid. Nanofluid.*, 6(5):679–692, 2009.

[8] J. P. du Plessis and S. Woudberg. Pore-scale derivation of the Ergun equation to enhance its adaptability and generalization. *Chem. Eng. Science*, 63:2576 2586, 2008.

[9] M. Gad-el Hak. *MEMS: Introduction and Fundamentals*. CRC Press, 2005.

[10] G. Gamrat, M. Favre-Marinet, S. Le Person, R. Bavière, and F. Ayela. An experimental study and modelling of roughness effects on laminar flow in microchannels. *J. Fluids Mech.*, 594: 399–423, 2008.

[11] H. Hasimoto. On the periodic fundamental solutions of the stokes equations and their application to viscous flow past a cubic array of spheres. *J. Fluid Mech.*, 5:317–328, 1959.

[12] H. Herwig, D. Gloss, and T. Wenterodt. A new approach to understanding and modelling the influence of wall roughness on friction factors for pipe and channel flows. *J. Fluid Mech.*, 613 (-1):35–53, 2008.

[13] Y. Hori. *Hydrodynamic lubrication*. Springer, 2006.

[14] F. A. Howes and S. Whitaker. The spatial averaging theorem revisited. *Chemical Engineering Science*, 40(8):1387 – 1392, 1985.

[15] S. G. Kandlikar, D. Schmitt, A. L. Carrano, and J. B. Taylor. Characterization of surface roughness effects on pressure drop in single-phase flow in minichannels. *Phys. Fluids*, 17(10): 100606, 2005.

[16] G. E. Karniadakis, A. Beskok, and N. R. Aluru. *Microflows and nanoflows: fundamentals and simulation*. Springer, 2005.

[17] M. Kaviany. *Principles of Heat Transfer in Porous Media*. Springer, 2nd ed. edition, 1999.

[18] S.A. Khuri. Stokes flow in curved channels. *J. Computational Appl. Math.*, 187(2):171 – 191, 2006. ISSN 0377-0427.

[19] C. Kleinstreuer and J. Koo. Computational analysis of wall roughness effects for liquid flow in micro-conduits. *J. Fluids Eng.*, 126(1):1–9, 2004.

[20] J. Koo and C. Kleinstreuer. Liquid flow in microchannels: experimental observations and computational analyses of microfluidics effects. *J. Micromech. Microeng.*, 13(5):568–579, 2003.

[21] G. M. Mala and D. Li. Flow characteristics of water in microtubes. *Int. J. Heat Fluid Flow*, 20(2):142 – 148, 1999.

[22] L. F. Moody. Friction factors for pipe flow. *ASME Trans.*, 66:671–683, 1944.

[23] G. M. Murphy. *Ordinary Differential Equations and Their Solutions*. D. Van Nostrand, 1960.

[24] A. Niavarani and N. V. Priezjev. The effective slip length and vortex formation in laminar flow over a rough surface. *Phys. Fluids*, 21:052105, 2009.

[25] J. Nikuradse. Laws of flow in rough pipes. Technical Report TM 1292, NACA, 1950.

[26] J. A. Ochoa-Tapia and S. Whitaker. Momentum transfer at the boundary between a porous medium and a homogeneous fluid–i. theoretical development. *Int. J. Heat Mass Transfer*, 38: 2635–2646, 1995.

[27] H. Ogata, K. Amano, M. Sugihara, and D. Okano. A fundamental solution method for viscous flow problems with obstacles in a periodic array. *J. Comput. Appl. Math.*, 152(1-2):411 – 425, 2003.

[28] A. D. Polyanin and V. F. Zaitsev. *Handbook of Exact Solutions for Ordinary Differential Equations*. Chapman & Hall/CRC Press, 2nd edition edition, 2003.

[29] K. Sarkar and A. Prosperetti. Effective boundary conditions for stokes flow over a rough surface. *J. Fluid Mech.*, 316(-1):223–240, 1996.

[30] W. F. Scaggs, R. P. Taylor, and H. W. Coleman. Measurement and prediction of rough wall effects on friction factor - uniform roughness results. *J. Fluids Eng.*, 110(4):385–391, 1988.

[31] P. N. Shankar. *Slow viscous flows: qualitative features and quantitative analysis using complex eigenfunction expansions*. World Scientific, 2007.

[32] A. D. Stroock, S. K. Dertinger, G. M. Whitesides, and A. Ajdari. Patterning flows using grooved surfaces. *Analyt. Chem.*, 74(20):5306–5312, October 2002.

[33] H. Struchtrup. *Macroscopic transport equations for rarefied gas flow: approximation methods in Kinetic Theory*. Springer, 2005.

[34] R. P. Taylor, H. W. Coleman, and Hodge B. K. Prediction of turbulent rough-wall skin friction using a discrete element approach. *J. Fluids Eng.*, 107:251257, 1985.

[35] S. C. Tung and M. L. McMillan. Automotive tribology overview of current advances and challenges for the future. *Trybol. Int.*, 37:517536, 2004.

[36] J. R. Valdés, M. J. Miana, J. L. Pelegay, J. L. Nú nez, and T. Ptz. Numerical investigation of the influence of roughness on the laminar incompressible fluid flow through annular microchannels. *Int. J. Heat Mass Transfer*, 50(9-10):1865 – 1878, 2007.

[37] J. R. Valdés, Mario J. Miana, Miguel Martínez, Leticia Gracia, and Thomas P'utz. Introduction of a length correction factor for the calculation of laminar flow through microchannels with high surface roughness. *Int. J. Heat Mass Transfer*, 51(17-18):4573 – 4582, 2008.

[38] F. J. Valdés-Parada, B. Goyeau, and J.A. Ochoa-Tapia. Jump momentum boundary condition at a fluid-porous dividing surface: derivation of the closure problem. *Chem. Eng. Science*, 62: 4045–4039, 2007.

[39] F. J. Valdes-Parada, J. A. Ochoa-Tapia, and J. Alvarez-Ramirez. On the effective viscosity for the darcy-brinkman equation. *Physica A*, 385:69–79, 2007.

[40] C.Y. Wang. Slow viscous flow between hexagonal cylinders. *Transp. Porous Media*, 47(1): 67–80, 2002.

[41] H. Wang and Y. Wang. Influence of three-dimensional wall roughness on the laminar flow in microtube. *Int. J. Heat Fluid Flow*, 28(2):220 – 228, 2007.

[42] S. Whitaker. Flow in porous media i: A theoretical derivation of Darcy's law. *Transp. Porous Med.*, 1(1):3–25, 1986.

[43] S. Woudberg and J. P. Du Plessis. Permeability prediction of cross-flow through 2D isotropic unidirectional fibre beds. *(Submitted)*, 2009.

[44] L. P. Yarin, A. Mosyak, and G. Hetsroni. *Fluid flow, heat transfer and boiling in microchannels*. Springer, 2009.

[45] D. Zwillinger. *Handbook of Differential Equations*. Academic Press, 1997.